Molecular Biology of the Cell
Vol. 16, 128–140, January 2005

Genetic Analysis of the Neuronal and Ubiquitous AP-3 Adaptor Complexes Reveals Divergent Functions in Brain[D]

E. Seong,[*] B. H. Wainer,[†] E. D. Hughes,[‡] T. L. Saunders,[‡] M. Burmeister,[*§] and V. Faundez[§‖¶]

[*]Mental Health Research Institute and Neuroscience Program and [‡]Department of Internal Medicine and Transgenic Animal Model Core, University of Michigan, Ann Arbor, MI 48109; and Departments of [†]Pathology and Laboratory Medicine and [‖]Cell Biology and the [¶]Center for Neurodegenerative Diseases, Emory University, Atlanta, GA 30322

Submitted October 13, 2004; Revised November 1, 2004; Accepted November 2, 2004
Monitoring Editor: Sandra Schmid

Neurons express adaptor (AP)-3 complexes assembled with either ubiquitous (β3A) or neuronal-specific (β3B) β3 isoforms. However, it is unknown whether these complexes indeed perform distinct functions in neuronal tissue. Here, we explore this hypothesis by using genetically engineered mouse models lacking either β3A- or β3B-containing AP-3 complexes. Somatic and neurological phenotypes were specifically associated with the ubiquitous and neuronal adaptor deficiencies, respectively. At the cellular level, AP-3 isoforms were localized to distinct neuronal domains. β3B-containing AP-3 complexes were preferentially targeted to neuronal processes. Consistently, β3B deficiency compromised synaptic zinc stores assessed by Timm's staining and the synaptic vesicle targeting of membrane proteins involved in zinc uptake (ZnT3 and ClC-3). Surprisingly, despite the lack of neurological symptoms, β3A-deficient mouse brain possessed significantly increased synaptic zinc stores and synaptic vesicle content of ZnT3 and ClC-3. These observations indicate that the functions of β3A- and β3B-containing complexes are distinct and divergent. Our results suggest that concerted nonredundant functions of neuronal and ubiquitous AP-3 provide a mechanism to control the levels of selected membrane proteins in synaptic vesicles.

INTRODUCTION

Membrane proteins reach their resident organelles by means of vesicle carriers that selectively sequester membrane protein cargo (Bonifacino and Glick, 2004). Central to membrane protein sorting and vesiculation processes is a family of cytosolic adaptor (AP) complexes that recognize sorting signals present on cargo proteins (Boehm and Bonifacino, 2001; Bonifacino and Traub, 2003; Robinson, 2004). Adaptors are made of four subunits or adaptins: a large α, γ, δ, or ε adaptin; a large β, a medium μ, and a small σ subunit. Numbers appended to the β, μ, or σ adaptin denote the adaptor complex to which the subunit belongs. Thus, for example, the adaptor complex 3 (AP-3) is assembled by a single copy of δ, β3, μ3, and σ3 adaptins. Diverse vesiculation mechanisms are accounted only in part by multiple adaptors. In mammalian cells, four adaptor complexes are localized to specific subcellular locations providing a first layer of diversity in the generation of distinct vesicle carriers (Boehm and Bonifacino, 2001; Bonifacino and Traub, 2003; Robinson, 2004). However, multiple isoforms in the subunits constituting individual adaptor complexes likely provide additional diversification to the membrane protein sorting and vesiculation mechanisms (Takatsu *et al*., 1998; Folsch *et al*., 1999, 2001, 2003).

The AP-3 complex is unique among adaptors because three of its subunits are encoded by two alternative genes: β3A/β3B, μ3A/μ3B, and σ3A/σ3B (Dell'Angelica *et al*., 1997a,b; Simpson *et al*., 1997). Of these subunits, β3B and μ3B are exclusively expressed in neurons, suggesting that they assemble AP-3 complexes devoted to neuron-specific sorting and vesiculation (Pevsner *et al*., 1994; Newman *et al*., 1995). Our knowledge about AP-3 function has been greatly illuminated by spontaneous AP-3 mouse mutations affecting two independent loci, *mocha* (Kantheti *et al*., 1998, 2003) and *pearl* (Feng *et al*., 1999). Loss of AP-3 in these mice leads to defective biogenesis of lysosomes and specialized secretory organelles, such as melanosomes, platelet-dense granules, lymphocyte cytotoxic granules (Dell'Angelica *et al*., 2000; Clark *et al*., 2003), and in neurons, synaptic vesicles (Kantheti *et al*., 1998, 2003; Salazar *et al*., 2004a,b).

Mocha affects δ adaptin, a unique AP-3 subunit expressed in all tissues and an obligatory component to all AP-3 complexes (Kantheti *et al*., 1998, 2003). Its absence leads to degradation of all the AP-3 subunits both in neuronal and nonneuronal tissues (Kantheti *et al*., 1998, 2003). In contrast, the *pearl* allele perturbs the β3A subunit, thus depleting AP-3 in all tissues except neurons, which still assemble AP-3 complexes carrying the neuronal-specific β3B isoform (Feng *et al*., 1999). *Pearl* and *mocha* mice share all their lysosomal and specialized secretory phenotypes except for those that depend on the assembly of synaptic vesicles, an organelle exclusively perturbed in the *mocha* allele. This divergence on the synaptic phenotypes associated with AP-3 deficiencies may derive from the fact that *pearl* neurons possess func-

Article published online ahead of print. Mol. Biol. Cell 10.1091/mbc.E04–10–0892. Article and publication date are available at www.molbiolcell.org/cgi/doi/10.1091/mbc.E04–10–0892.

[D] The online version of this article contains supplemental material at MBC Online (http://www.molbiolcell.org).

[§] Corresponding authors. E-mail addresses: margit@umich.edu; faundez@cellbio.emory.edu.

tional β3B-containing AP-3 complexes. Yet, this alone does not explain whether neurons selectively require β3B-containing AP-3 complexes (neuronal AP-3), or whether β3A- and β3B-containing AP-3 complexes are functionally interchangeable in neuronal tissue as is the case in nonspecialized fibroblastic cell types (Peden *et al*., 2002). In vitro reconstitution of synaptic-like microvesicle biogenesis supports the first hypothesis because formation of these vesicles requires neuronal AP-3 complexes (Faundez *et al*., 1998; Blumstein *et al*., 2001). However, whether neuronal β3B-containing AP-3 fulfills unique functions in the biogenesis of brain synaptic vesicles and regulates presynaptic functions remains largely unexplored. In this manuscript, we investigated whether β3B-neuronal AP-3 complexes mediate unique neuron-specific functions that cannot be accomplished by β3A-containing AP-3. We tested this hypothesis by using genetically engineered mouse strains lacking neuronal or ubiquitous AP-3 generated by ablation of the β3B and β3A subunits, *Ap3b2*$^{-/-}$ and *Ap3b1*$^{-/-}$, respectively. Analysis of the subcellular distribution of AP-3, the synaptic zinc stores, and the targeting of AP-3–dependent synaptic vesicle cargoes ZnT3 and CIC-3 (Salazar *et al*., 2004a,b) indicated that the functions of both AP-3 complexes were distinct and divergent. Our results suggest that concerted nonredundant functions of neuronal and ubiquitous AP-3 provide a mechanism to control levels of membrane proteins in synaptic vesicles.

MATERIALS AND METHODS

Animals

The *Ap3b1*$^{-/-}$ mouse line congenic on C57BL/6J was kindly donated by Dr. S. Mansour (University of Utah, Salt Lake City, UT) (Yang *et al*., 2000) and then bred in-house. *Ap3b2*$^{-/-}$ animals were generated by directly targeting C57BL/6 and continued breeding on the same genetic background. Most animals for our experiments were obtained from matings of heterozygous males and females. Control animals used were *Ap3b2*$^{+/+}$ littermates of *Ap3b2*$^{-/-}$ animals. *Mocha* mice were originally obtained from The Jackson Laboratory (Bar Harbor, ME) and then bred in-house, also as heterozygotes. All animal procedures were approved by the University of Michigan and Emory University Committees on Use and Care of Animals.

Ap3b2 Targeting and Ap3b2$^{-/-}$ *Mouse Generation*

To generate *Ap3b2*$^{-/-}$ mice on a C57BL/6 (B6) genetic background for comparison to *Ap3b1*$^{-/-}$ mice, we targeted *Ap3b2* in B6-derived (Bruce4) embryonic stem (ES) cells (Kontgen *et al*., 1993) as well as in 129S1/SvImJ (129)-derived (CJ7) ES cells (Swiatek and Gridley, 1993). Targeting frequency and germ line transmission from both ES cell lines have been previously compared for this construct (Seong *et al*., 2004).

The targeting vectors for both 129 and B6 targeting were prepared using the pflox vector (Chui *et al*., 1997). To target a large region of *Ap3b2*, we first screened 129 and B6 bacterial artificial chromosome (BAC) libraries (CITB-CJ7 and RPCI-23, respectively; Research Genetics, Huntsville, AL). From resulting BACs identified in each library, two identical targeting vectors were created by subcloning the target region, exons 5–12 of *Ap3b2*, from each of the coisogenic BACs into the pflox vector. After electroporation of the targeting vector, ES cells were screened by genomic polymerase chain reaction (PCR) followed by Southern blot analysis of PCR-positive clones. Further Southern blot analyses and PCR from both ends were performed to verify that the selected ES cells have a properly targeted allele without affecting neighboring genomic regions. *Ap3b2*$^{-/-}$ animals were obtained on three genetic backgrounds: 129, B6, and (129 × B6)F2. However, to compare the most similar genetic backgrounds, only *Ap3b2*$^{-/-}$ mice on C57BL/6 were used for the data presented here.

Northern blots were prepared as described previously (Bomar *et al*., 2003). ^{32}P-labeled antisense RNA probes were prepared by in vitro transcription using Maxiscript (Ambion, Austin, TX) from *Ap3b1* and *Ap3b2* reverse transcription (RT)-PCR fragments with the additional following T7 sequence at the 5′ of reverse primers: TAA TAC GAC TCA CTA TAG GGA G. Ap3b1 and Ap3b2 RT-PCR primers are Ap3b1mF3161 (ACT TCA CTC CCT CCA TGA TCC TC), Ap3b1mR3498 (TGC CAG ATG GAA GGG CTA TTA TT), Ap3b2mF2874 (CAG CCA ACT TCC AGC TGT GC), and Ap3b2mR3143 (TCC TCC CTG CAA ACC TGT ACT C).

Open Field Test

Individual mice were placed into a white nontransparent chamber 33.5 × 36.5 cm in size, and activity was recorded for 100 min. Horizontal locomotion of each mouse was determined using Ethovision software (Noldus, Amsterdam, The Netherlands). Statistical analysis was performed with SPSS 11.0. Statistical analyses were performed using the unpaired *t* test and analysis of variance followed by Bonferroni correction.

Antibodies

Monoclonal antibody (mAb) to synaptophysin (SY38) and polyclonal antibody to MAP2 were purchased from Chemicon International (Temecula, CA). mAb to SV2 (10H4) was a gift of Dr. R. Kelly (University of California, San Francisco, San Francisco, CA). Anti-116-kDa subunit of the vacuolar ATPase was purchased from Synaptic Systems (Göttingen, Germany). Affinity-purified antibodies directed against ClC-3 were a gift from Dr. D. J. Nelson (University of Chicago, Chicago, IL) (Huang *et al*., 2001). Affinity-purified polyclonal antibody against ZnT3 has been described previously (Salazar *et al*., 2004b). mAb against AP-3 δ (SA4) was obtained from Developmental Studies Hybridoma Bank at the University of Iowa (Iowa City, IA) (Peden *et al*., 2004). mAb to β3B (βNAP) was purchased from BD Transduction Laboratories (Lexington, KY). Polyclonal pan-β3 antibody that recognizes both β3A and β3B, and polyclonal pan-σ3 have been described previously (Faundez *et al*., 1998; Salem *et al*., 1998). Polyclonal antipeptide antibodies against β3B were described in Blumstein *et al*. (2001).

Primary Cultures of Cortical Neurons

Cultures were generated from 16-d-old mouse embryos. *Ap3b1*$^{-/-}$, *Ap3b2*$^{-/-}$, *mocha*, and control mating cages were set up at the same time, and embryos were processed simultaneously. The morning that the vaginal plug occurred was defined as day 1. Because homozygous *Ap3b2*$^{-/-}$ and *mocha* animals are subfertile, homozygous males were mated to heterozygous females to obtain homozygous embryos. *Ap3b1*$^{-/-}$ and *mocha* embryos were identified by the delayed eye pigmentation phenotype. *Ap3b2*$^{-/-}$ embryos were morphologically indistinguishable; thus, entire litters were individually processed and genotyped later.

Primary cultures of cortical neurons were performed according to the method described by Meberg and Miller (2003) with some modifications. Briefly, both cortical hemispheres from each embryo were isolated and dissociated with trypsin, and cells were plated at 10,000 cells/cm^2 in Neurobasal medium with 10% fetal bovine serum (FBS), 1× 100 U/ml penicillin and 100 μg/ml streptomycin (PS). After 12 h, the FBS-containing medium was replaced with Neurobasal medium supplemented with B27, L-glutamine, 1× PS. 5-Fluorouracil deoxyribonucleoside (1 μM) was added 4 d after plating, and cells were fed twice weekly thereafter with the same B27-supplemented Neurobasal medium. Cortical neurons were grown at 37°C in 5% CO_2 on coverslips coated with poly-D-lysine (Sigma-Aldrich, St. Louis, MO) in 24-well plates. All cell culture reagents were purchased from Invitrogen (Carlsbad, CA). Cells were used after 4–19 d in vitro (DIV).

Immunocytochemistry and Confocal Microscopy

Cells were washed twice in phosphate-buffered saline (PBS) for 5 min. After washing, cells were fixed for 20 min in 4% paraformaldehyde and processed for immunofluorescence. Fixed cells were permeabilized in blocking buffer (0.02% saponin in PBS, 2% bovine serum albumin, and 1% fish skin gelatin) for 30 min, and then incubated with primary antibodies for 90 min. After washing three times with blocking buffer, each time 15 min, cells were incubated with secondary antibody for 60 min. Secondary antibodies used were Alexa-conjugated goat anti-mouse 488 and/or goat anti-rabbit 594. Cells were then rinsed and mounted in Prolong Gold (Invitrogen). Specimens were viewed using a FluoView 500 confocal microscope (Olympus, San Diego, CA) coupled to HeNeG and Argon ion lasers. Alexa-488 and Alexa-594 were excited with the Argon laser tuned at 488 nm and the HeNeG laser tuned at 543 nm, respectively. Images were acquired using FluoView 4.3 software (Olympus). The emission filters used were BA505–525 and BA610IF. Images were viewed and acquired using UplanApo 20×/0.7, 60×/1.4 oil, or 100×/1.4 oil objective. To compare *Ap3b1*$^{-/-}$, *Ap3b2*$^{-/-}$, *mocha*, and control neurons, all images were captured at the same time and threshold values.

Timm's Staining

Adult *mocha*, *Ap3b1*$^{-/-}$, *Ap3b2*$^{-/-}$, and control mice were used for Timm's staining. Timm's staining was performed according to the method by Sloviter (1982) with some modifications. After an anesthetic overdose (pentobarbital, 60 mg/kg i.p.), all animals were transcardially perfused as follows: 1× PBS, pH 7.2 (Invitrogen) for 3 min, 0.37% sulfide solution, pH 7.2, for 5 min, and 4% paraformaldehyde in 1× PBS for 3 min. The brains were removed, postfixed for 3–5 h, and left overnight in 25% sucrose in 0.1 M phosphate buffer, pH 7.4. Coronal vibratome sections (40 μm in thickness) were mounted on slides and allowed to dry. Sections were developed in the dark for 45 min in a solution consisting of 250 ml of 50% gum arabic, 40 ml of sodium citrate buffer, 120 ml of 5.7% hydroquinone, and 2 ml of 17% silver nitrate. Slides were then rinsed in distilled water for 5 min, dehydrated, and coverslipped.

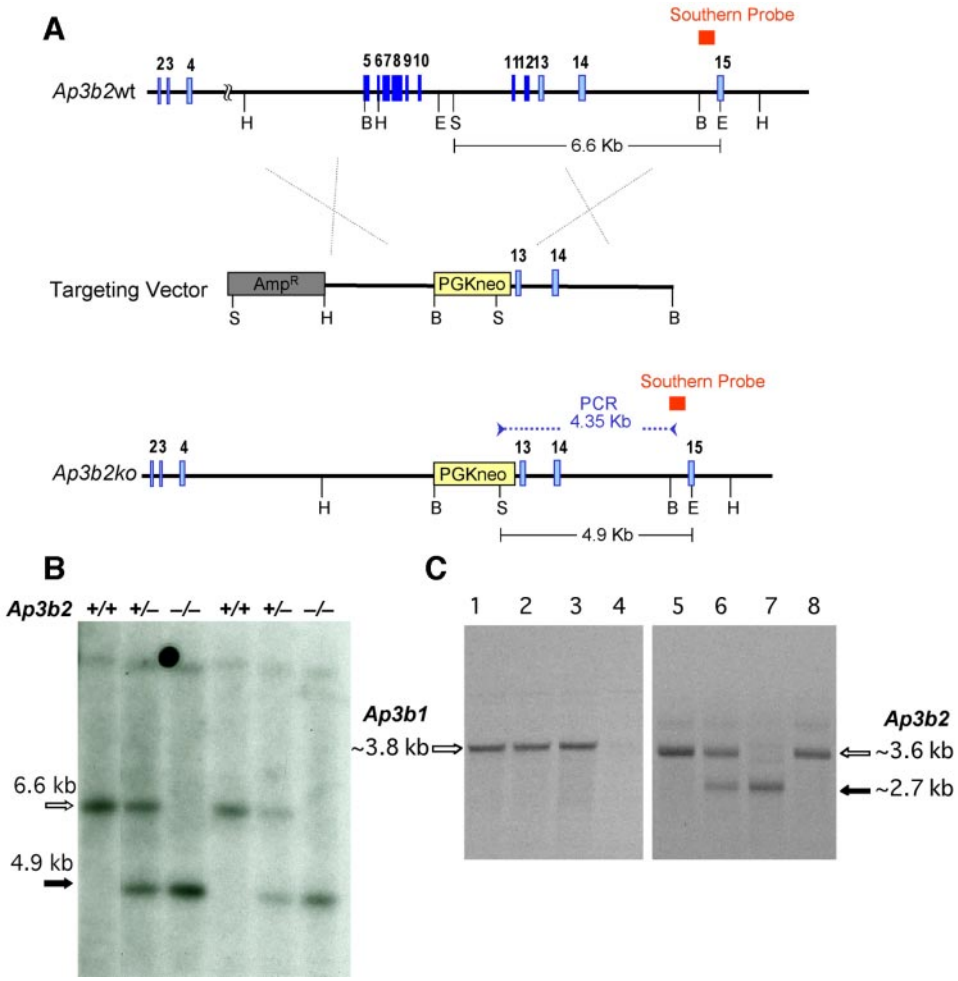

Figure 1. Generation of *Ap3b2*$^{-/-}$ mice by gene-targeting. (A) Schematic diagram showing the *Ap3b2* locus (wt), the targeting vector, and the targeted *Ap3b2* allele (ko). All coding exons in the region are depicted as light or dark boxes numbered on the top. The dark blue boxes represent targeted exons 5–12, which are replaced by the PGKneo cassette in the *Ap3b2*ko allele. E, *Eco*RV; H, *Hind*III; B, *Bam*HI; S, *Spe*I. (B) Southern blot analysis of *Ap3b2* locus. Genomic DNA from wild-type (+/+), heterozygous (+/−), and homozygous mutant (−/−) animals was digested with *Eco*RV and *Spe*I. The probe location is shown as a red box in Figure 1A. The *Ap3b2*ko allele is detected as a 4.9-kb and the wild-type allele as 6.6-kb fragment. The first three lanes are animals from a 129 line, and the last three lanes from a B6 line. (C) *Ap3b1* and *Ap3b2* Northern blot analyses. Lanes 1 and 5, wild-type control. Lanes 2 and 6, *Ap3b2*$^{+/-}$. Lanes 3 and 7, *Ap3b2*$^{-/-}$. Lane 4 and 8: *Ap3b1*$^{-/-}$. The hybridization probe for the left blot is specific for *Ap3b1* mRNA. Only wild-type *Ap3b1* mRNA is visible and is indicated by a white arrow. The hybridization probe for the right blot is specific for *Ap3b2* mRNA. The wild-type and the targeted transcript (2.7 kb) are marked by a white and a black arrow, respectively.

Sections were viewed at 6.3× under transillumination by using a Leica MZ FL III stereomicroscope (Leica Microsystems, Bannockburn, IL). Images were captured on a DKC5000 digital camera (Sony, Tokyo, Japan) and acquired using Adobe Photoshop (Adobe Systems, San Jose, CA).

Immunohistochemistry

Animals were treated similarly, except that sulfide was omitted from the perfusion solution. Brains were then sliced coronally and embedded in paraffin. To ensure identical processing, slices containing control, *Ap3b1*$^{-/-}$, and *Ap3b2*$^{-/-}$ hippocampi were included in the same block and sectioned together (8 μm in thickness). Antigens were retrieved by microwave treatment in 10 mM citrate buffer, pH 6, for 10 min. All stainings were performed in duplicate in at least two independent experiments. Primary antibody incubations were carried out overnight at 4°C, and immunocomplexes were detected by species-specific Vectstain avidin-biotinylated enzyme complex kit (Vector Laboratories, Burlingame, CA) according to manufacturer's instructions. ZnT3 antibody was used at 1/200; serial dilutions up to 1/1000 gave identical results.

Morphometric Analyses

Fluorescence intensity determinations were performed using MetaMorph software (Universal Imaging, Downingtown, PA). Tiff files of single optical sections obtained with FluoView 4.3 software were imported directly into MetaMorph. Processes and cell bodies were identified in the MAP-2 channel, outlined, and the average delta fluorescence intensity of at least four randomly selected processes per neuron was measured. Images were collected from two independent experiments totaling 36 wild-type, 33 *Ap3b1*$^{-/-}$, 34 *Ap3b2*$^{-/-}$, and 11 mocha neurons. Specific δ antibody fluorescence intensity was determined by subtracting the average fluorescence intensity obtained in *mocha* neurons from wild-type, *Ap3b1*$^{-/-}$, and *Ap3b2*$^{-/-}$ values.

Timm's staining images were captured in color using Photoshop software. Tiff files were converted to gray scale and inverted to obtain "negatives" of the brain section images by using Adobe Photoshop 7. Timm's deposits showed up as a white signal, which was quantified using MetaMorph software. Average intensities were obtained from two areas of the brain cortex and from the stratum oriens and radiatum of the hippocampi. A total of 19 wild-type (3 mice), 20 *Ap3b1*$^{-/-}$ (3 mice), 29 *Ap3b2*$^{-/-}$ (4 mice), and 13 *mocha* (2 mice) brain sections obtained in three independent experiments were analyzed.

Cell Fractionation, Immunoprecipitation, and Western Blot Analysis

Frozen brains of *Ap3b1*$^{-/-}$, *Ap3b2*$^{-/-}$, and control animals were pulverized to a fine powder by using porcelain mortars under a continuous supply of liquid nitrogen. Extracts were thawed at 4°C in 5 volumes of buffer A (150 mM NaCl, 10 mM HEPES, pH 7.4, 1 mM EGTA, and 0.1 mM $MgCl_2$ plus Complete antiprotease mixture; Salazar *et al.*, 2004a). Homogenates were sedimented at 1000 × *g* for 10 min to generate S1 supernatants. S1 were further fractionated at 27,000 × *g* for 45 min to obtain high-speed supernatants, which were resolved in glycerol velocity gradients (5–25%) prepared in intracellular buffer at 218,000 × *g* for 75 min in a SW55 rotor (Beckman Coulter, Fullerton, CA). Gradient fractions were analyzed by immunoblot, and immunoreactivity was revealed by enhanced chemiluminescence. Immunoreactive bands were quantified using NIH Image 1.62 software as described previously (Salazar *et al.*, 2004b).

Immunoprecipitation was performed with polyclonal pan-σ3 or monoclonal δ antibodies prebound to protein G-Sepharose, as described previously (Faundez and Kelly, 2000; Salazar *et al.*, 2004b).

Other Procedures

Protein concentration was determined by Bradford reagent (Bio-Rad, Hercules, CA). Data are expressed as average ± SE. Statistical analysis was performed using nonpaired, two-tailed *t* test.

RESULTS

β3B-deficient Mice Generated by Gene-targeting of Ap3b2

Neurons abundantly express AP-3 complexes assembled with either the ubiquitous or the neuronal-specific β3 isoforms (Newman *et al*., 1995; Dell'Angelica *et al*., 1997b). However, it has not been determined whether the function of β3A- and β3B-containing AP-3 complexes is redundant in neurons, a specialized secretory cell. To test this hypothesis, we targeted *Ap3b2* exons 5 through 12 and removed one-third of the *Ap3b2* coding region near the N terminus (Figure 1A) to create a β3B-deficient mouse model. The normal β3B protein consists of 1082 amino acids, whereas the targeted gene encodes an aberrantly short polypeptide consisting of the first 120 amino acids followed by 63 extra amino acid residues. The *Ap3b2* gene was disrupted in both CJ7 (129S1/SvImJ-derived) and Bruce4 (C57BL/6-derived) ES cell lines (Seong *et al*., 2004). Properly targeted ES cell lines and their germline transmission in animals were screened and confirmed by both PCR (our unpublished data) and Southern blot analysis (Figure 1B). CJ7 ES cell-derived *Ap3b2*$^{-/-}$ lines were bred to C57BL/6J, and *Ap3b2*$^{-/-}$ animals were on a mixed F2 genetic background of 129S1/SvImJ (129) and C57BL/6 (B6) strains. By targeting in the Bruce4 ES cell line, a different *Ap3b2*$^{-/-}$ line was created on a B6 background. Although the major phenotypes of *Ap3b2*$^{-/-}$ mice were consistent regardless of the genetic background, we used *Ap3b2*$^{-/-}$ mice on B6 for comparisons with *Ap3b1*$^{-/-}$ mice on the same genetic background. *Ap3b1*$^{-/-}$ mice were initially generated in ES cells from two different 129 substrains (Yang *et al*., 2000), but they have been repeatedly (>8 generations) backcrossed to B6, resulting in an almost pure B6 genetic background. We used *Ap3b1*$^{-/-}$ instead of *pearl* mice because they carry a null allele for β3A, whereas *pearl* mice carry a hypomorphic allele (Yang *et al*., 2000; Peden *et al*., 2002). Disruption of the *Ap3b1* or *Ap3b2* loci was demonstrated either by the absence of transcripts or by the generation of aberrant transcripts, respectively. Transcripts of the targeted *Ap3b1* allele were absent (Figure 1C, lane 4). However, the targeted *Ap3b2* mRNA was transcribed into a smaller mRNA of ~2.7 kb, with exons 5 through 12 replaced with the neo cassette from the vector (Figure 1C, lane 7). Although the aberrant mRNA is as stable as the wild-type, RT-PCR analysis confirmed that its sequence did indeed contain an early stop codon due to a frame shift mutation as well as the deletion; as predicted from our targeting vector. Importantly, the amount of *Ap3b1* transcript was not altered in *Ap3b2*$^{-/-}$ mice, and likewise, *Ap3b1*$^{-/-}$ mice had the normal amount of *Ap3b2* transcript (Figure 1C, compare lanes 5 and 8, and 1 and 3, respectively). These results demonstrate that there is no dramatic compensatory increase of either transcript in the absence of the other.

AP-3 Complex Assembly in β3A and β3B Adaptin Deficiencies

We further explored the effects of engineered β3B and β3A deficiencies upon brain β3 expression levels by using a panel of antibodies that selectively recognize either the β3B subunit, both β3 subunits, or AP-3 subunits common to both AP-3 complexes, δ and σ3A-B (Figure 2). Brain homogenates from wild-type (control), β3A- (*Ap3b1*$^{-/-}$), and β3B-deficient mice (*Ap3b2*$^{-/-}$) were probed with monospecific anti-β3B antibodies (Figure 2A, lanes 1–6) or with an antibody recognizing both β3 subunits (Figure 2A, lanes 7–9). β3B adaptin was readily detectable in both control and β3A-deficient (*Ap3b1*$^{-/-}$) mouse brain homogenates (Figure 2A, lanes 1–2 and 4–5). In contrast, both β3B antibodies fail to detect β3B protein in β3B-deficient extracts (*Ap3b2*$^{-/-}$; Figure 2A, lanes 3 and 6). We did not detect compensatory changes of β3B protein expression levels in β3A-deficient brains (Figure 2A, compare lanes 1 and 2, 4 and 5). Importantly, the remaining β3A adaptin present in β3B-deficient mice was detected with the β3 antibody recognizing both β3 subunits (Figure 2A, lane 9); thus, confirming the specific nature of the β3 deficiencies.

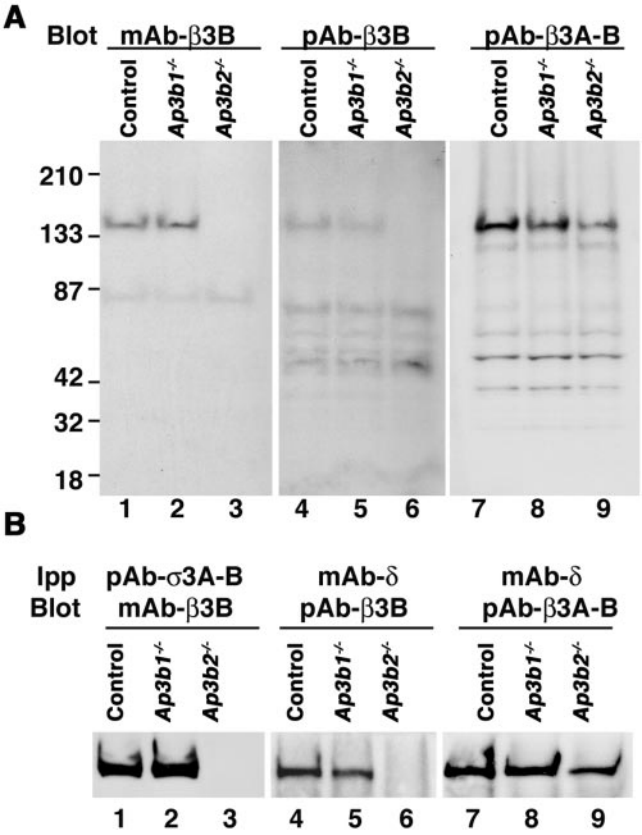

Figure 2. Assembly of β3A- and β3B-containing complexes in *Ap3b1*$^{-/-}$ and *Ap3b2*$^{-/-}$ brain. (A) Western blots of control, *Ap3b1*$^{-/-}$, and *Ap3b2*$^{-/-}$ brain homogenates were probed with either monoclonal β3B (lanes 1–3) or polyclonal β3B (lanes 4–6) antibodies. Both antibodies specifically recognize a band of ~140 kDa, which is absent in β3B-deficient *Ap3b2*$^{-/-}$ homogenates. Anti β3A-B polyclonal antibody (lanes 7–9) recognizes both β3A and β3B. Note that β3B in *Ap3b1*$^{-/-}$ and β3A in *Ap3b2*$^{-/-}$ homogenates exist in comparable amounts. Smaller nonspecific bands indicate that the same amount of total protein was loaded for each brain homogenate. (B) Brain homogenates were immunoprecipitated with either σ3 polyclonal (lanes 1–3) or δ mAb (lanes 4–9). Immunocomplexes were resolved by SDS-PAGE, transferred to membranes, and probed with monoclonal β3B (lanes 1–3), polyclonal β3B (lanes 4–6), or β3A-B polyclonal antibodies (lanes 7–9). Absence of β3B in lanes 3 and 6 ensures the specificity of both β3B antibodies.

To evaluate whether β3B and β3A present in *Ap3b1*$^{-/-}$ and *Ap3b2*$^{-/-}$ brain tissue were assembled into whole heterotetramers, we tested whether β3B- and β3A-containing AP-3 complexes could be immunoprecipitated with antibodies against δ and σ3 adaptins. These two AP-3 subunits do not directly bind β3 (Peden *et al*., 2002). However, δ and σ3 adaptins indirectly associate with β3 in the context of holotetramers (Peden *et al*., 2002). AP-3 complexes containing β3B were immunoprecipitated with σ3 antibodies, from both control and *Ap3b1*$^{-/-}$ brain extracts (Figure 2B, lanes

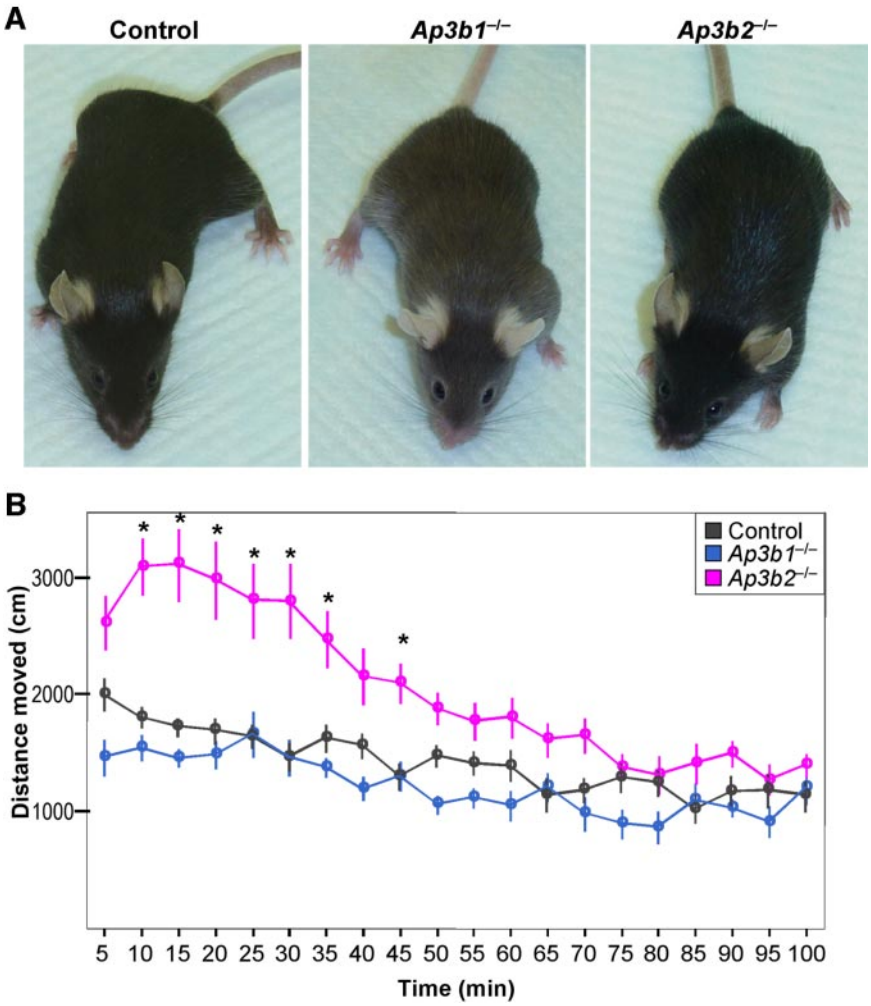

Figure 3. Distinctive phenotypes of isoform specific AP-3 deficiencies. (A) $Ap3b1^{-/-}$ mice have lighter coat and skin (ear, tail) colors, but $Ap3b2^{-/-}$ mice have normal pigmentation, indistinguishable from the control. (B) Open field test. Ethovision animal behavior analysis software was used to automatically measure horizontal movement. Distance moved for every 5 min is plotted for 100 min. $Ap3b2^{-/-}$ animals were twice as active during the first 30 min. After 50 min, their activity was not significantly different from control (*$p < 0.01$). Eleven control, 10 $Ap3b1^{-/-}$, and 11 $Ap3b2^{-/-}$ mice were tested.

1–2). These complexes were absent from $Ap3b2^{-/-}$homogenates (Figure 2B, lane 3). Similarly, δ antibodies immunoprecipitated β3B present in control and $Ap3b1^{-/-}$ homogenates (Figure 2B, lanes 4–5), demonstrating that the neuronal-specific β3 subunit was incorporated into AP-3 complexes. β3A-containing complexes were still present in β3B-deficient brain extracts (Figure 2B, lane 9). Thus, the lack of either β3A- or β3B-AP-3 does not appreciably perturb the other adaptor isoform. In summary, our results demonstrate that $Ap3b1^{-/-}$ and $Ap3b2^{-/-}$ mouse brains selectively lack β3A- and β3B-containing AP-3 complexes, without detectable compensatory changes.

Distinct Phenotypes Distinguish $Ap3b1^{-/-}$ and $Ap3b2^{-/-}$ Mice

The absence of ubiquitous and neuronal AP-3 in *mocha* leads to pigment dilution and neurological disorders such as locomotor hyperactivity (Kantheti *et al.*, 1998). To assess the tissue penetrance of these phenotypes in isoform-specific deficiencies, we analyzed pigmentation and open field activity in $Ap3b1^{-/-}$ and $Ap3b2^{-/-}$ mice. As predicted from its selective expression in neurons (Newman *et al.*, 1995), removal of β3B did not affect coat color (Figure 3A). $Ap3b2^{-/-}$ mice possessed normal black coat color, indistinguishable from the control. In contrast, $Ap3b1^{-/-}$ mice display a light gray coat color thus confirming that only ubiquitous AP-3 is involved in skin melanosome biogenesis. On the other hand, horizontal locomotor activity in response to handling was significantly increased in $Ap3b2^{-/-}$, whereas it was normal in $Ap3b1^{-/-}$ mice (Figure 3B). During the first 30 min in the open field, $Ap3b2^{-/-}$ mice exhibited twofold higher locomotion than control (Figure 3B), which gradually receded to nearly control values. Multiple behavioral and electroencephalographic analyses further demonstrated a normal neurological phenotype in $Ap3b1^{-/-}$ mice but complex neurological and behavioral impairments, including tonic-clonic seizures, in $Ap3b2^{-/-}$ mice (Seong and Burmeister, unpublished data). These observations indicate that the hyperactivity observed in *mocha* is due to the absence of neuronal AP-3 complexes. Overall, these results indicate that neuronal and nonneuronal phenotypes are selectively triggered by isoform-specific adaptor deficiencies.

Neuronal and Ubiquitous AP-3 Complexes Possess Distinct Subcellular Distribution in Neurons

Functionally distinct adaptors possess characteristic and unique subcellular distribution both in polarized and nonpolarized cells (Gan *et al.*, 2002; Folsch *et al.*, 2003; Robinson, 2004). Thus, we hypothesized that divergence in the function of ubiquitous (β3A) and neuronal (β3B) AP-3 could be manifested as differential distribution of isoforms within neurons. We took advantage of primary cultures of embry-

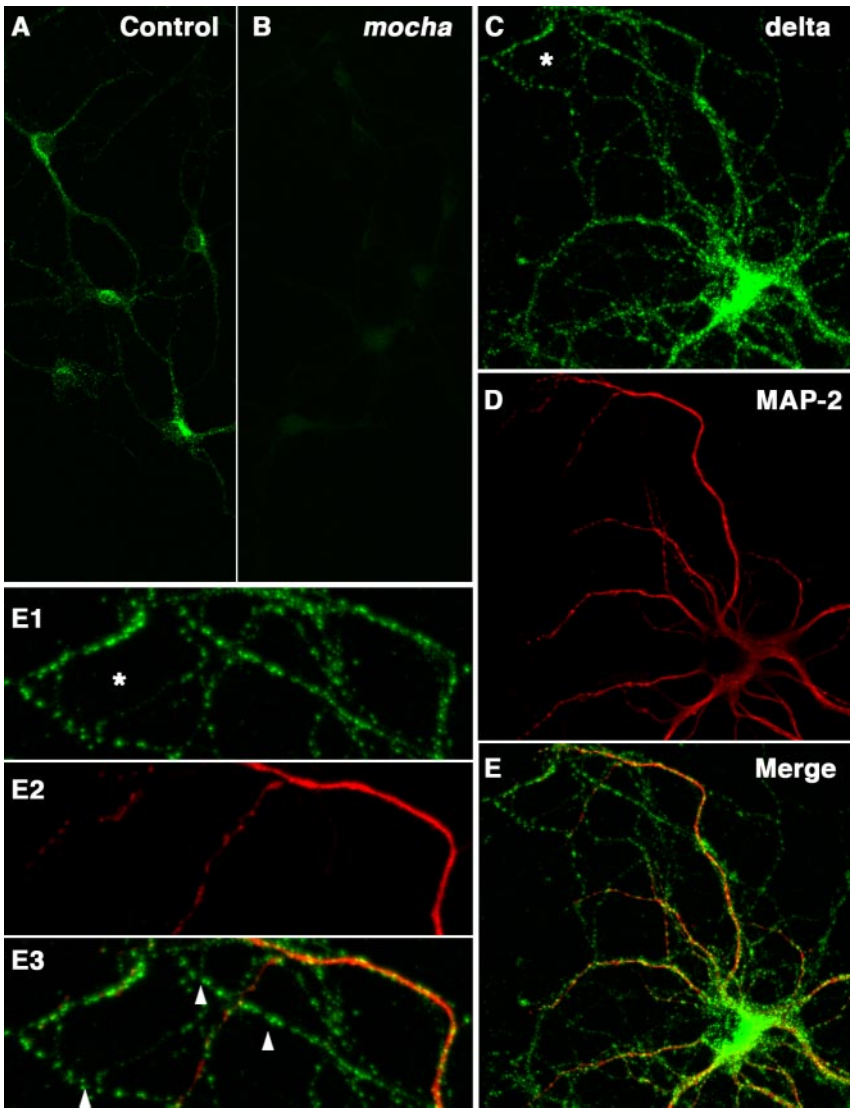

Figure 4. AP-3 is present in dendritic and axonal projections. Control (A) and *mocha* (B) neurons (8 DIV) were stained with δ mAb. Negligible signal is detected in mocha neurons evidencing the specificity of the staining procedure. (C) Neurons (19 DIV) were costained with δ (C, E1) and MAP-2 (D, E2) antibodies to reveal dendritic processes (100× lens). Note that AP-3 is similarly present in both dendritic (MAP-2 positive) and axonal processes (MAP-2 negative, arrowheads). Asterisk marks the region amplified in E1–E3. Arrowheads point to MAP-2–negative processes.

onic neurons derived from *Ap3b1*$^{-/-}$ or *Ap3b2*$^{-/-}$ mouse forebrains as cellular systems exclusively containing neuronal or ubiquitous AP-3, respectively. These neuronal cultures possess a branched and polarized morphology where subcellular domains can be easily identified by cytoskeletal markers (Caceres *et al*., 1986).

Primary neuronal cultures were immunostained with δ antibodies to highlight the neuronal AP-3 complexes present in *Ap3b1*$^{-/-}$ cells or the ubiquitous AP-3 present in *Ap3b2*$^{-/-}$ neurons. We selected a single antibody to avoid differences that could emerge from disparity in antigen–antibody complex formation by using the isoform specific β3 antibodies. Moreover, and in contrast with the δ mAb, both β3 antibodies were unsatisfactory in fixed cells. We first determined the specificity of the δ antibody staining (Peden *et al*., 2004) by using wild-type and *mocha* brain primary cultured neurons. *Mocha* neurons do not express functional δ subunits, making them an ideal control. Delta antibody decorated abundant AP-3 puncta present in neuronal cell bodies as well as in all processes (Figure 4A). In contrast, specific fluorescent signal was ablated in *mocha* cell bodies and process (Figure 4B), demonstrating the specificity of this antibody.

AP-3 has been described in cell bodies, neuronal processes, and nerve terminals by using a variety of antibodies, neuronal cell types, and species (Darnell *et al*., 1991; Newman *et al*., 1995; Simpson *et al*., 1996; Zakharenko *et al*., 1999). Thus, we explored whether AP-3 selectively decorated axons and/or dendrites in primary cultured mouse neurons. Cultured neurons develop polarized axons and dendrites, cell domains, which can be distinguished by the presence of MAP-2 in dendrites (Caceres *et al*., 1986). Neurons were cultured for 19 DIV to allow the development of extensive and interconnected processes (neuropil) and double labeled with δ and MAP-2 antibodies (Figure 4, C–E). AP-3–positive organelles were detected in cell bodies, MAP-2–positive (dendrites) and MAP-2–negative (axons) processes. There were no appreciable differences in the AP-3 content and distribution between axons and dendrites (Figure 4, E1–E3), suggesting that AP-3 was equally segregated between these neuronal domains. To explore whether neuronal and ubiquitous AP-3 were differentially distributed in neurons, we double labeled wild-type, *Ap3b1*$^{-/-}$, and *Ap3b2*$^{-/-}$ neurons with δ and MAP-2 antibodies and imaged cells by confocal microscopy (Figure 5). Wild-type and β3B-containing neurons (*Ap3b1*$^{-/-}$, Figure 5, D–F) showed prominent AP-3

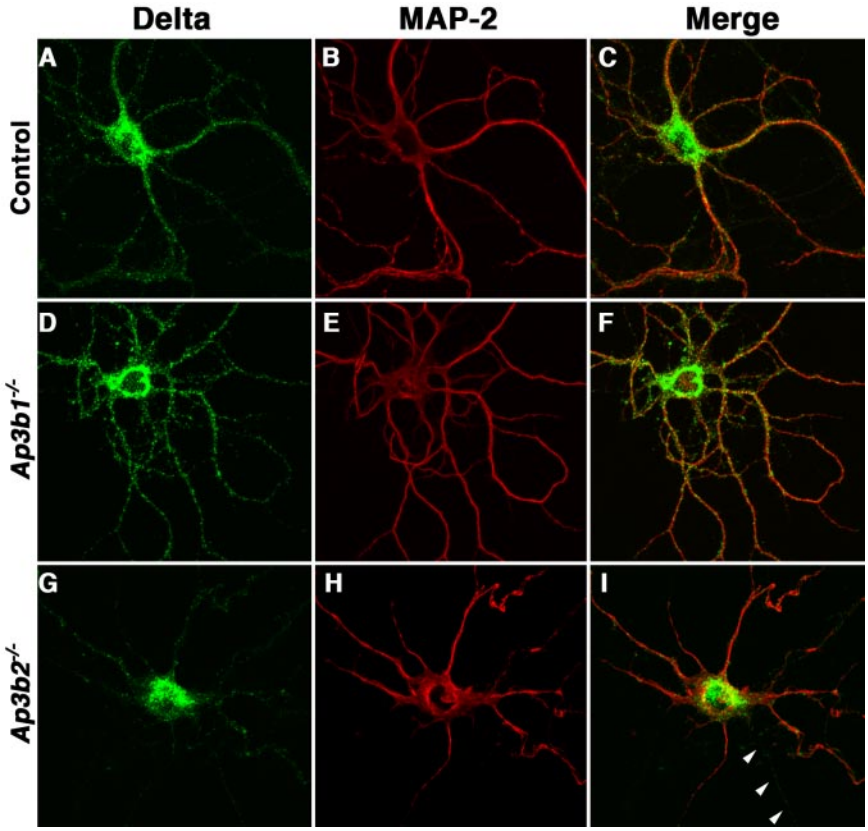

Figure 5. Localization of neuronal and ubiquitous AP-3 in neuronal processes. Control, *Ap3b1*$^{-/-}$, and *Ap3b2*$^{-/-}$, 19 DIV neurons were costained with delta (A, D, and G) and MAP-2 (B, E, and H) antibodies. Control and *Ap3b1*$^{-/-}$neurons have similar intracellular AP-3 distribution patterns both in cell bodies and processes. In contrast, *Ap3b2*$^{-/-}$ cells have decreased AP-3 staining in processes. By inspection of *Ap3b2*$^{-/-}$ neurons we noticed that axons and dendrites were similarly compromised (see arrowheads in I).

labeling in cell bodies, MAP-2–positive and –negative processes. In contrast, neurons lacking neuronal AP-3 (*Ap3b2*$^{-/-}$, Figures 5, G–I, and 6A) consistently showed a dramatically decreased staining of all processes despite the fact that the cell body AP-3 content seemed normal. We confirmed these observations by quantitative analysis of AP-3 fluorescence intensity by using MetaMorph software (Figure 6B). There were no significant differences in fluorescence intensity among cell bodies, irrespective of both their genetic background and the time that cells were differentiated in vitro (DIV) (Figure 6B). In contrast, neuronal AP-3–deficient cells (*Ap3b2*$^{-/-}$) contained 2.6 times less AP-3 in their processes when differentiated for 7 d ($p < 0.001$ n = 98 wild-type and 95 *Ap3b2*$^{-/-}$ processes analyzed). This phenotype was even more pronounced in cells differentiated for 15 d (15 DIV). *Ap3b2*$^{-/-}$ neuronal processes contained 4.2-fold less AP-3 than their wild-type counterpart (Figure 6B, $p < 0.001$ n = 38 wild-type and 56 *Ap3b2*$^{-/-}$ processes analyzed). Thus, these results not only confirm our observations in 7 DIV neurons, but they also rule out that the lack of AP-3 in *Ap3b2*$^{-/-}$ cell processes is due to a developmental delay in the export of ubiquitous AP-3 to cell processes.

In summary, these results indicate that, at steady state, mature neurons preferentially target neuronal AP-3 to cell processes in a nonpolarized manner. The distinct targeting of neuronal and ubiquitous AP-3 strongly supports the hypothesis that AP-3 isoforms perform divergent functions in neurons.

Presynaptic Mechanisms Are Impaired in Neuronal AP-3–deficient Brain

The presence of neuronal AP-3 in axons (Figures 4, C–E, and 6A), nerve terminals, and its reported function in the biogenesis of synaptic vesicles (Newman *et al*., 1995; Faundez *et al*., 1998; Zakharenko *et al*., 1999; Blumstein *et al*., 2001; Salazar *et al*., 2004b) prompted us to explore whether presynaptic mechanisms were affected in *Ap3b1*$^{-/-}$ and *Ap3b2*$^{-/-}$ brains. To test this hypothesis, we explored the content of histochemically reactive ionic zinc. Ionic zinc is stored exclusively in synaptic vesicles (Frederickson, 1989) by the action synaptic-specific zinc transporter ZnT3 (Palmiter *et al*., 1996; Cole *et al*., 1999), an AP-3–interacting molecule (Salazar *et al*., 2004b). Moreover, ZnT3 (Cole *et al*., 1999) or AP-3 (*mocha*) (Kantheti *et al*., 1998; Kantheti *et al*., 2003) genetic deficiencies severely compromise synaptic zinc stores, thus making histochemically reactive zinc an unparalleled reporter of synaptic AP-3 function.

We performed Timm's staining in control and mutant mice brain sections to assess the histochemically reactive presynaptic zinc pools. We used *mocha* brain sections as controls. As previously described, Timm's staining was prominent in discrete cortex layers and in different regions of the hippocampus (Figure 7A) (Frederickson, 1989; Frederickson and Danscher, 1990). Histochemically reactive zinc was substantially reduced in all these regions in *mocha* brain (Figure 7D), thus validating Timm's staining as a tool to assess neuronal AP-3 synaptic phenotypes. We focused our analysis in the brain cortex and the stratum oriens (Figure 7A, area 3) and radiatum of the hippocampal formation (Figure 7A, area 4). Timm's staining deposits were reduced in all brain areas of *Ap3b2*$^{-/-}$ brains, although the phenotype was not as pronounced as in *mocha* brain. Quantification of the Timm's staining by using MetaMorph software showed that in all areas of *Ap3b2*$^{-/-}$ mouse brain there was on average a 25% reduction in Timm's staining intensity (n = 27 brain sections in three independent experiments).

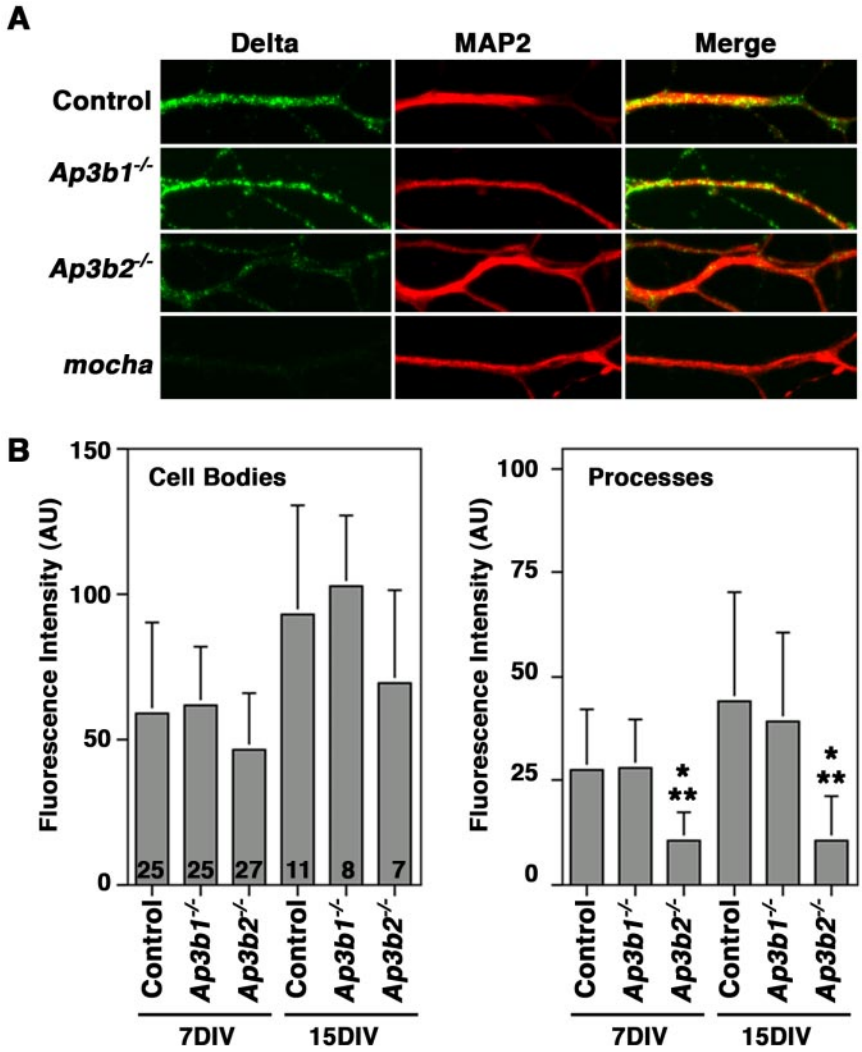

Figure 6. Neuronal AP-3 complex is preferentially targeted to neuronal processes. Control, *Ap3b1*$^{-/-}$, *Ap3b2*$^{-/-}$, and *mocha* 7 and 15 DIV neurons were costained with delta and MAP-2 antibodies. (A) Depicts representative images of neuronal processes from 15 DIV neurons, note the reduced AP-3 levels in *Ap3b2*$^{-/-}$ processes and the absence of signal in the mocha projections. (B) AP-3 fluorescence intensity analysis in neuronal cell bodies and processes. Fluorescence intensity from *mocha* cell bodies and processes was subtracted from control, *Ap3b1*$^{-/-}$, and *Ap3b2*$^{-/-}$ values. There are no statistically significant differences in the cell body AP-3 content among different mouse genotypes. In contrast, processes of *Ap3b2*$^{-/-}$ contain reduced levels of AP-3 both at 7 and 15 DIV. Asterisk and double asterisk denote $p < 0.001$ for control/*Ap3b2*$^{-/-}$ and *Ap3b1*$^{-/-}$/*Ap3b2*$^{-/-}$ respectively. The n values are described in *Materials and Methods* and as numbers at the bottom of the bars. AU = Arbitrary units.

The most dramatic differences were observed in the CA1 stratum oriens with 62 ± 5% of the control values found in *Ap3b2*$^{-/-}$ brains (n = 12). Surprisingly, in the absence of ubiquitous AP-3 (*Ap3b1*$^{-/-}$), we observed a significant increase of 12% in the histochemically reactive zinc pools ($p < 0.045$), in the cortex as well as the hippocampus (n = 20), thus supporting the hypothesis that the functions carried out by the ubiquitous and neuronal AP-3 are divergent.

Decreased synaptic ionic zinc content in *mocha* synapses is associated with reduced ZnT3 protein levels in brain tissue as well as in synaptic vesicles (Salazar *et al*., 2004b). To explore whether the changes in Timm's staining observed in *Ap3b1*$^{-/-}$ and *Ap3b2*$^{-/-}$ were paralleled by changes in ZnT3 levels, we determined the ZnT3 content by immunocytochemistry in hippocampal brain sections. As we described previously (Salazar *et al*., 2004a), there was a drastic reduction in the total ZnT3 protein levels in *mocha* mouse hippocampus compared with control brain sections (Supplementary Figure 1, compare G and H). In contrast, we did not detect differences in the ZnT3 levels and distribution in *Ap3b1*$^{-/-}$ and *Ap3b2*$^{-/-}$ hippocampi (Supplementary Figure 1, A–F). Identical results were obtained with serial dilutions of ZnT3 antibody (our unpublished data). This suggests that rather than global changes in ZnT3 protein content, the changes in synaptic zinc observed in *Ap3b1*$^{-/-}$ and *Ap3b2*$^{-/-}$ hippocampi may represent modifications not detectable by immunocytochemical techniques. These results suggest that in the subcellular distribution of membrane proteins involved in the synaptic vesicle zinc uptake is differentially affected in *Ap3b1*$^{-/-}$ and *Ap3b2*$^{-/-}$ mouse models.

ZnT3 and ClC-3 Targeting to Small Vesicles Are Differentially Modified in Ap3b1$^{-/-}$ *and Ap3b2*$^{-/-}$ *Brains*

Synaptic vesicle ionic zinc uptake is critically dependent on two AP-3–trafficked transmembrane proteins, ZnT3 (Cole *et al*., 1999) and the synaptic vesicle chloride channel ClC-3 (Salazar *et al*., 2004a). The targeting of both proteins into synaptic vesicles is impaired after pharmacological or genetic (*mocha*) perturbation of AP-3 function (Salazar *et al*., 2004a,b). Thus, we hypothesized that the changes in synaptic zinc observed in *Ap3b1*$^{-/-}$ and *Ap3b2*$^{-/-}$ brain were associated with corresponding modifications in the content of ZnT3 and ClC-3 in *Ap3b1*$^{-/-}$ and *Ap3b2*$^{-/-}$ synaptic vesicles. To address this question, we analyzed the targeting of these two proteins to synaptic vesicles from control, *Ap3b1*$^{-/-}$, and *Ap3b2*$^{-/-}$ brains. Synaptic vesicles can be isolated from high-speed supernatants fractionated in velocity glycerol gradients. Velocity sedimentation discriminates vesicles by size, resolving large membranes from small syn-

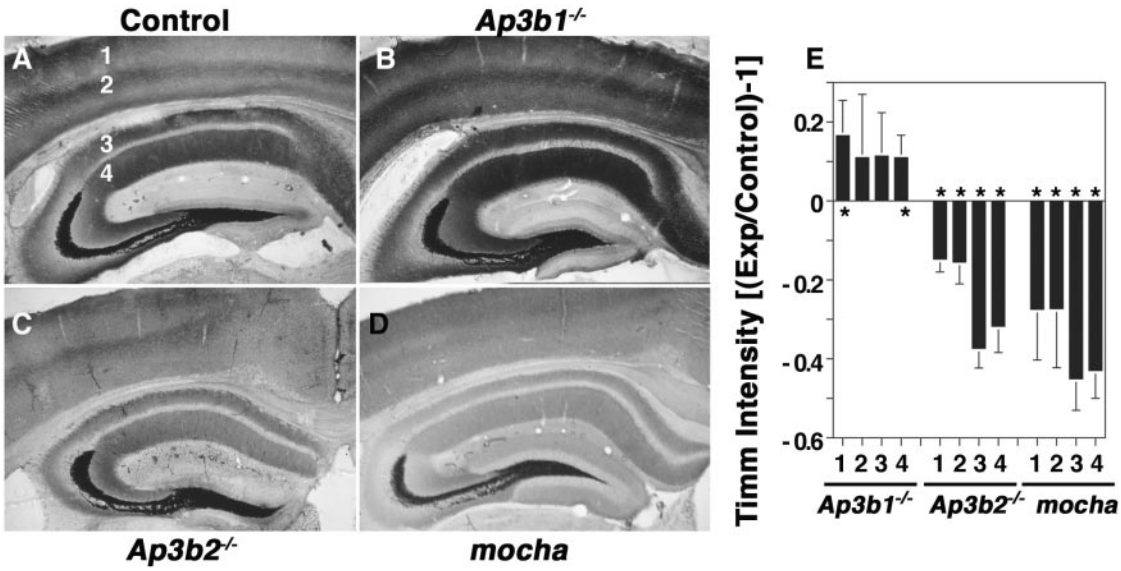

Figure 7. Selective reduction of vesicular zinc in the absence of neuronal AP-3. Histochemically reactive zinc was assessed by Timm's staining of control (A), *Ap3b1*$^{-/-}$ (B), *Ap3b2*$^{-/-}$ (C), and *mocha* (D) coronal brain sections. (A) Values 1 and 2 correspond to distinct layers of the brain cortex, and 3 and 4 correspond to the stratum oriens and radiatum of the hippocampus. *Mocha* possesses prominently reduced Timm's stain. *Ap3b2*$^{-/-}$ hippocampus and cortex have reduced Timm's deposits. Note the increase in *Ap3b1*$^{-/-}$ cortex and stratum radiatum. (E) Quantitative analysis of Timm's deposits. Control sections were assigned a 0 value. Increases are seen as values >0, decreased Timm's staining correspond to values <0. Asterisks mark statistically significant differences (at least $p < 0.05$). The n values are described in *Materials and Methods*.

aptic vesicles, which sediment as a symmetric peak in the middle of the gradient (fractions 7–9) (Salazar *et al*., 2004a,b). We monitored synaptic vesicle marker content and its distribution along gradients to assess both targeting and whether these proteins were present in synaptic vesicles, respectively. We selected membrane proteins whose targeting to synaptic vesicles is affected by the *mocha* allele (ZnT3, ClC-3) and contrasted their behavior to AP-3–independent cargoes (synaptophysin, SV2, and the 116-kDa subunit of the vacuolar ATPase) (Salazar *et al*., 2004a,b). All of membrane proteins analyzed cosedimented as a symmetric peak around fraction 8 in control brain membranes (Figure 8). On the contrary, the AP-3 cargoes did not cosediment with the AP-3–independent markers in *Ap3b2*$^{-/-}$ brains (Figure 8). One-fifth of the ZnT3 protein contained in the membranes resolved by glycerol sedimentation was present at the peak synaptic vesicle fraction from wild-type membranes (fraction 8 = 20.5 ± 1.63%, n = 5), whereas we observed a 40% decrease in *Ap3b2*$^{-/-}$ membranes ($p < 0.001$, n = 5). These results are consistent with the hypothesis that ZnT3 targeting to synaptic vesicles was impaired in the absence of neuronal AP-3. Remarkably, the absence of ubiquitous AP-3 (*Ap3b1*$^{-/-}$) rather than reducing ZnT3 in synaptic vesicles doubled its content (ZnT3 in fraction 8 = 41.2 ± 15.4%, $p < 0.001$, n = 5). The increased content of an AP-3 cargo in *Ap3b1*$^{-/-}$ synaptic vesicles was not restricted to ZnT3. Similarly, we observed a 1.8-fold increase in the ClC-3 synaptic vesicle content in ubiquitous AP-3–deficient *Ap3b1*$^{-/-}$ membranes (control 19.2 ± 3.5%, *Ap3b1*$^{-/-}$ 34.6 ± 5.2%, n = 4, $p < 0.05$). ClC-3 targeting to small vesicles was also altered in the absence of neuronal AP-3. ClC-3 content in *Ap3b2*$^{-/-}$ small vesicles was increased, although the membranes containing ClC-3 migrated into the gradient faster than synaptic vesicles (fraction 6). In wild-type membranes, only 9.9 ± 2.3% (n = 4) of the total ClC-3 contained in the overall gradient is present in fraction 6, yet in neuronal AP-3 deficiency this fraction contains 33.1 ± 5.5% (n = 4, $p < 0.01$), providing evidence of defective ClC-3 targeting in *Ap3b2*$^{-/-}$ neurons. The changes in the content and distribution of AP-3 cargoes (ZnT3 and ClC-3) observed in the isotype-selective AP-3 deficiencies were specific. The distribution and synaptic vesicle content of the AP-3–independent cargoes, synaptophysin (Sphysin), SV2, and the vacuolar ATPase subunit remained unaffected in *Ap3b1*$^{-/-}$ and *Ap3b2*$^{-/-}$ brains.

Collectively, these data are consistent with the hypothesis that selective defects in AP-3 cargo targeting contribute to the synaptic zinc phenotypes observed in *Ap3b1*$^{-/-}$ and *Ap3b2*$^{-/-}$ brains. Moreover, they indicate that the functions of the neuronal and ubiquitous AP-3 complexes in neurons are divergent, despite the fact that both regulate synaptic vesicle protein composition.

DISCUSSION

Neurons possess AP-3 adaptors carrying either β3A or β3B (Newman *et al*., 1995; Dell'Angelica *et al*., 1997b). Absence of both β3 subunits, such as in the *mocha* allele (Kantheti *et al*., 1998), leads to neurological manifestations, a phenotype absent in mice deficient just in β3A (*pearl*) (Feng *et al*., 1999). An attractive hypothesis to explain this phenotypic difference is that β3B-AP-3 performs a specific role in neuronal physiology. However, *mocha* and *pearl* alleles do not discriminate whether β3B-containing AP-3 complexes perform functions unique to neurons, or whether β3A- and β3B-containing AP-3 complexes are functionally interchangeable in neuronal tissue. We addressed this question by using mouse strains selectively lacking the ubiquitous AP-3 subunit β3A (*Ap3b1*$^{-/-}$) or the neuronal-specific β3 subunit β3B (*Ap3b2*$^{-/-}$). Herein, we demonstrate that AP-3 complexes assembled with β3A or β3B perform preferentially distinct and divergent roles in neuronal-specific sorting and vesicu-

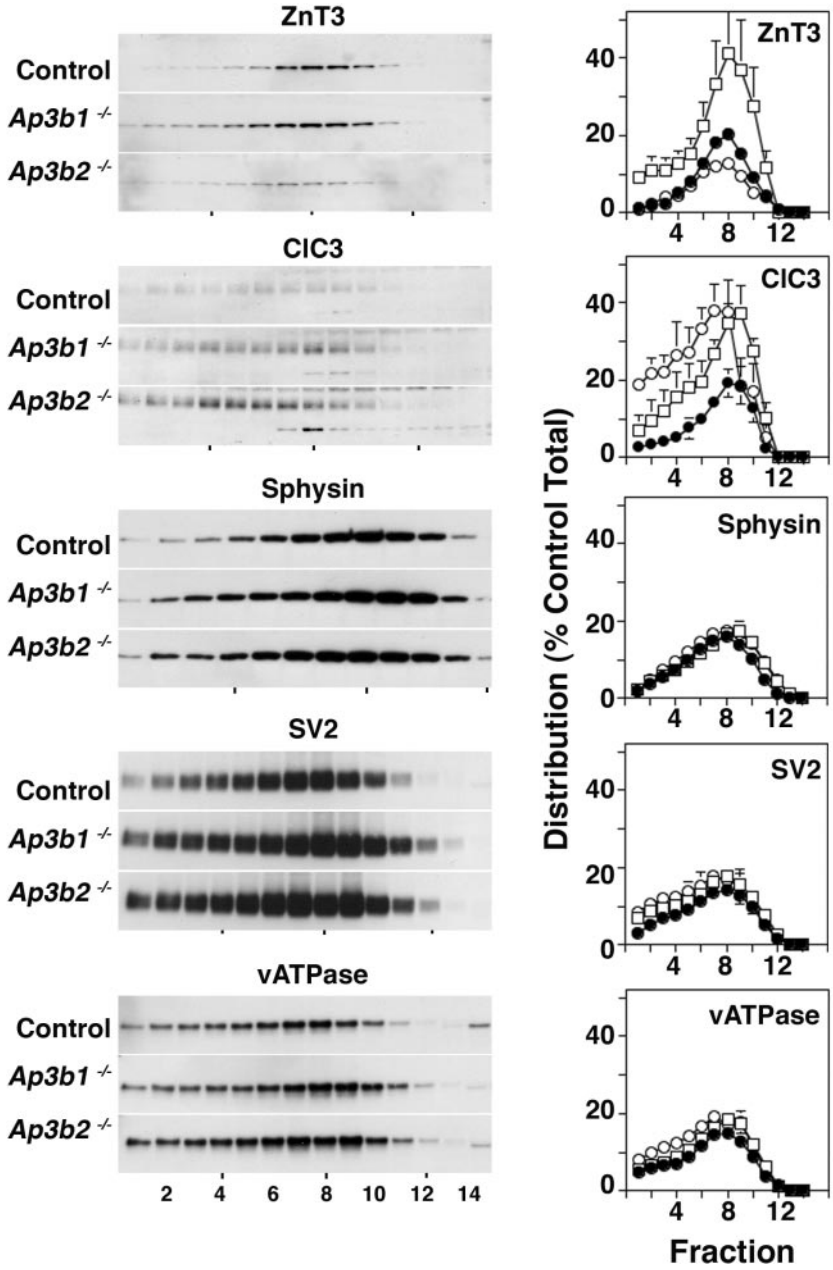

Figure 8. Targeting of synaptic vesicle proteins to small vesicles in *Ap3b1*$^{-/-}$ and *Ap3b2*$^{-/-}$ brains. High-speed supernatants (S2) from control, *Ap3b1*$^{-/-}$, and *Ap3b2*$^{-/-}$ brain homogenates were fractionated in 5–25% glycerol gradients to resolve small vesicles (peak at fractions 7–9). Synaptic vesicle protein levels across gradients were determined by immunoblot by using antibodies against: ZnT3 (A), ClC-3 (B), synaptophysin (Sphysin, C), SV2 (D), and vacuolar ATPase (vATPase, E). Only ZnT3 and ClC-3 sedimentation pattern and their protein levels are altered in *Ap3b1*$^{-/-}$ and *Ap3b2*$^{-/-}$ brain vesicles. (F–J) Normalized protein distribution of ZnT3 (n = 5), ClC-3 (n = 4), and Sphysin (n = 3), SV 2 (n = 2), and vATPase (n = 2): Each fraction value is a figure normalized to the total amount of control samples. Closed circles represent control vesicles, and open squares and circles correspond to *Ap3b1*$^{-/-}$ and *Ap3b2*$^{-/-}$ vesicles, respectively. ZnT3 (F) increases in the absence of ubiquitous AP-3, and decreases in absence of neuronal AP-3. Total protein level of ClC-3 (G) increases in both *Ap3b1*$^{-/-}$ and *Ap3b2*$^{-/-}$ S2. The increased ClC-3 in *Ap3b1*$^{-/-}$ S2 still has the same distribution shape as control S2, whereas the increased ClC-3 in *Ap3b2*$^{-/-}$ is redistributed to membranes bigger than synaptic vesicles. Note the peak of open circle is shifted toward left. Fraction 1 corresponds to the bottom in all gradients (A–E).

lation mechanisms. Four lines of evidence support our conclusion. First, we have successfully segregated the pigment dilution and hyperactivity phenotypes observed in the *mocha* mouse (Kantheti *et al*., 1998) with deficiencies of the ubiquitous and neuronal-specific AP-3, respectively. Second, β3A- and β3B-containing AP-3 complexes are differentially distributed in neuronal cell bodies and processes of cultured neurons. Ubiquitous and neuronal AP-3 distribute similarly in neuronal cell bodies. Nevertheless, β3B-containing AP-3 is approximately fourfold more abundant than β3A-AP-3 in axons and dendrites. Third, histochemically reactive synaptic vesicle zinc is selectively decreased in β3B deficiency, yet it increases in β3A-null cells. Finally, targeting of two AP-3 synaptic vesicle cargo proteins, ZnT3 and ClC-3, is selectively impaired in β3B-deficient neurons. In contrast, ZnT3 and ClC-3 content are increased at least twofold in synaptic vesicle fractions from β3A-deficent neurons.

Interpretation of the neuronal phenotypes in *Ap3b1*$^{-/-}$ and *Ap3b2*$^{-/-}$ rests on the assumption that the changes induced by each genetic ablation are constrained to just one AP-3 isoform. Our data provide evidence supporting this notion. Neuronal AP-3 present in *Ap3b1*$^{-/-}$ mouse brain is assembled into complexes containing δ and σ3 subunits. These heterotetramers can be recruited to membranes because β3B-AP-3 is clearly discernible in puncta rather than the cytoplasm of neurons. This line of thought is further supported by the increased content of synaptic vesicle specific AP-3 cargoes (ZnT3 and ClC-3) in small vesicle populations from *Ap3b1*$^{-/-}$ neurons. Thus, based on the quaternary structure, presence on membranes, and effects upon synaptic vesicle protein targeting, neuronal complexes present on the *Ap3b1*$^{-/-}$ neurons are capable of sorting and vesiculation. Together, these results support the hypothesis that specialized sorting and vesiculation mechanisms ful-

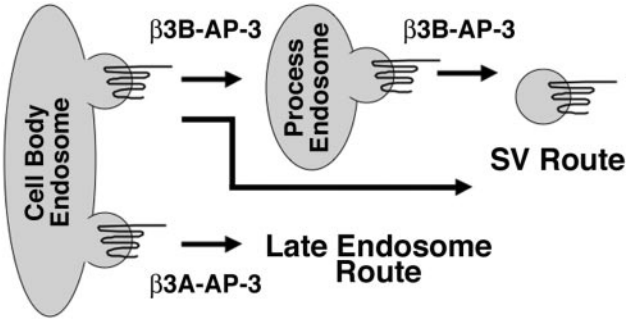

Figure 9. Neuronal and Ubiquitous AP-3 act on distinct vesiculation pathways. Diagram depicts a model of β3A- and β3B-containing adaptor function in neurons. Perikarial (cell body) and axodendritic (processes) endosomes are portrayed. These compartments differ in the content of ubiquitous β3A-AP-3. The multispanning membrane proteins represent a synaptic vesicle-specific cargo similarly recognized by β3A- or β3B-containing adaptors. In cell body endosomes, this protein can be diverted into two routes, whereas in axo-dendritic endosomes it only follows the synaptic vesicle (SV) route. In the absence of β3A, *Ap3b1*$^{-/-}$, the synaptic vesicle cargo is sorted only into the neuronal specific route. Alternative pathways of synaptic vesicle protein sorting such as the AP-2–dependent mechanism are not represented for clarity.

filled by neuronal AP-3 cannot be efficiently replaced by β3A-AP-3 adaptors.

Histochemically reactive ionic zinc detected with Timm's staining mainly reports zinc pools present in synaptic vesicles (Frederickson, 1989). This vesicular pool requires the presence of a synaptic vesicle-specific transporter, ZnT3 (Palmiter *et al*., 1996), a membrane protein trafficked to synaptic vesicles by AP-3 (Kantheti *et al*., 1998; Salazar *et al*., 2004b). ZnT3$^{-/-}$ brains completely lack histochemically reactive vesicular zinc (Cole *et al*., 1999), thus demonstrating that this transporter is central to generate synaptic zinc pools. Although the decreased Timm's staining in β3B null as well as *mocha* brain was predicted by our hypothesis, the increased level of synaptic zinc in β3A-deficient brain was a revelation. This change in synaptic zinc likely is mechanistically linked with the concomitant increment in the synaptic vesicle ZnT3 and ClC-3 content. Both membrane proteins control vesicular zinc uptake (Cole *et al*., 1999; Salazar *et al*., 2004a). How can β3A and β3B deficiencies trigger opposing synaptic zinc phenotypes? In nonneuronal cells, ClC-3 targeting to late endosome/lysosome compartments is sensitive to the *mocha* allele (Salazar *et al*., 2004a), thus indicating that ClC-3 is recognized by ubiquitous β3A-containing AP-3. Therefore, if β3A-containing adaptors are incapable of distinguishing synaptic vesicle from nonsynaptic vesicle cargoes, then a reasonable hypothesis to explain the phenotypes observed in *Ap3b1*$^{-/-}$ mouse brain is that both AP-3 isoforms compete for synaptic vesicle membrane proteins (Figure 9). Thus, ZnT3 or ClC-3 may have two pathways to follow. Either they would be included in a β3A-AP3–generated vesicle in route to late endosomal compartments, or they would be sorted into a β3B-AP-3–generated vesicle to be delivered to synaptic vesicle pools (Figure 9). These divergent fates could be particularly prominent in neuronal cell bodies where β3A and β3B are abundantly represented, but less prominent in axons and dendrites where neuronal AP-3 is the predominant adaptor isoform (Figure 9). This model is consistent with the phenotypes observed in *Ap3b1*$^{-/-}$, *Ap3b2*$^{-/-}$, and *mocha* mice.

A puzzling observation is why ZnT3 and ClC-3 phenotypes are dissimilar in the *Ap3b2*$^{-/-}$ background, with ClC-3 being targeted to larger membranes and its levels increased whereas ZnT3 levels are decreased, yet the transporter is present in normal size vesicles. A possible explanation may derive from the fact that in neurons ClC-3 is targeted to synaptic vesicles and likely to lysosomes (Stobrawa *et al*., 2001; Salazar *et al*., 2004a), whereas in nonneuronal cells it is routed to lysosomes (Li *et al*., 2002). In contrast, ZnT3 has been reported only in synaptic vesicles (Wenzel *et al*., 1997). Thus, in the absence of neuronal AP-3, ClC-3 may accumulate in organelles distinct to those where ZnT3 may be present. To properly answer this question, additional factors need to be considered, such as the participation of the other neuronal AP-3 isoform μ3B (Blumstein *et al*., 2001), and the possibility that hierarchical and differential interactions may occur between other nonAP-3 adaptors, multiple sorting signals present in cargo proteins, and post-translational modifications affecting the sorting of some of these cargoes (Salazar and Faundez, unpublished observations).

An intriguing question is how β3 isoforms contribute to selective sorting and vesiculation. Tyrosine-based sorting signal recognition is carried out by μ3 subunits (Bonifacino and Traub, 2003), whereas the dileucine sorting signal is recognized by δ-σ3 (Janvier *et al*., 2003). μ3A and μ3B preferentially bind tyrosine-based sorting motifs (Ohno *et al*., 1998), suggesting that this subunit could contribute to the sorting selectivity of the neuronal and ubiquitous AP-3. Because β3 subunits assemble into β3/μ3 dimers (Peden *et al*., 2002), selective sorting of synaptic vesicle cargo could result from a preferential association of β3B/μ3B. However, two-hybrid analysis indicates that μ3B bind β3A but not β3B (Peden *et al*., 2002). Alternatively, the hinge-ear domains of both β3 subunits could play a role in recruiting accessory molecules or cargo-specific modular adaptors as in the case of β-arrestin (Laporte *et al*., 2000; Kim and Benovic, 2002; Laporte *et al*., 2002) or ARH (He *et al*., 2002; Mishra *et al*., 2002) in AP-2–mediated vesiculation. The relevance of these β3 domains is corroborated by β3A chimeras where the ear domain of β3A is replaced by the β2 adaptin ear. This hybrid adaptor complex is unable to rescue AP-3–deficient phenotypes (Peden *et al*., 2002). A complementary mechanism to explain β3A- or β3B- differences in cargo recognition and vesiculation could rely on the adaptors being in different domains of the neuron. This possibility is particularly attractive in light of the differential distribution of neuronal and ubiquitous AP-3 among cell bodies and axo-dendritic compartments. Interestingly, the AP-1 β1 subunit ear domain interacts with the motor kif13A modulating subcellular distribution and sorting function of AP-1 (Nakagawa *et al*., 2000). Although direct interactions of AP-3 with cytoskeletal motors have not been reported, recent evidence suggests that intermediate filaments regulate AP-3 function (Styers *et al*., 2004) and that AP-3 might regulate positioning of organelles in cytotoxic lymphocytes (Clark *et al*., 2003). Thus, a viable yet not exclusive mechanism to account for specialized functions of neuronal AP-3 may in part derive from spatial segregation of the adaptor complexes into distinct neuronal domains.

Taken collectively, our data indicate that in neurons ubiquitous and neuronal AP-3 complexes participate in distinct and divergent sorting and vesiculation processes. We propose that concerted opposing functions of neuronal and ubiquitous AP-3 provide a mechanism to control synaptic vesicle protein composition.

While this article was under review, Nakatsu *et al*. (2004) reported the characterization of an *Ap3m2* knockout mouse, which is also hyperactive and prone to seizures. Nakatsu *et al*. (2004) also reported electrophysiological changes attributed to missorting of the vesicular GABA transporter. Whether *Ap3m2* and *Ap3b2* knockout mice are otherwise similar in behavior or in cellular distribution of AP-3 complexes remains to be seen.

ACKNOWLEDGMENTS

We thank Jamee Bomar (University of Michigan) for help with animal care, Inderjeet Saluja for help with primary neuron culture protocols, and Jennifer Kearney for help with Timm's staining procedures. We thank Suzi Mansour (University of Utah) for the gift of the Ap3b1 knockout mice. We thank Colin Stewart (National Cancer Institute) for the gift of Bruce4 ES cells and Tom Gridley (The Jackson Laboratory) for the gift of CJ7 ES cells. This work was supported by grants from the National Institutes of Health, NS42599 (to V. F.) and NS032130 (to M. B.). The University of Michigan Transgenic Animal Model Core is supported by the University of Michigan Center for Organogenesis and the Michigan Technology Tri-Corridor (grant 085P1000815).

REFERENCES

Blumstein, J., Faundez, V., Nakatsu, F., Saito, T., Ohno, H., and Kelly, R. B. (2001). The neuronal form of adaptor protein-3 is required for synaptic vesicle formation from endosomes. J. Neurosci. *21*, 8034–8042.

Boehm, M., and Bonifacino, J. S. (2001). Adaptins: the final recount. Mol. Biol. Cell *12*, 2907–2920.

Bomar, J. M., *et al*. (2003). Mutations in a novel gene encoding a CRAL-TRIO domain cause human Cayman ataxia and ataxia/dystonia in the jittery mouse. Nat. Genet. *35*, 264–269.

Bonifacino, J. S., and Glick, B. S. (2004). The mechanisms of vesicle budding and fusion. Cell *116*, 153–166.

Bonifacino, J. S., and Traub, L. M. (2003). Signals for sorting of transmembrane proteins to endosomes and lysosomes. Annu. Rev. Biochem. *72*, 395–447.

Caceres, A., Banker, G. A., and Binder, L. (1986). Immunocytochemical localization of tubulin and microtubule-associated protein 2 during the development of hippocampal neurons in culture. J. Neurosci. *6*, 714–722.

Chui, D., Oh-Eda, M., Liao, Y. F., Panneerselvam, K., Lal, A., Marek, K. W., Freeze, H. H., Moremen, K. W., Fukuda, M. N., and Marth, J. D. (1997). Alpha-mannosidase-II deficiency results in dyserythropoiesis and unveils an alternate pathway in oligosaccharide biosynthesis. Cell *90*, 157–167.

Clark, R. H., Stinchcombe, J. C., Day, A., Blott, E., Booth, S., Bossi, G., Hamblin, T., Davies, E. G., and Griffiths, G. M. (2003). Adaptor protein 3-dependent microtubule-mediated movement of lytic granules to the immunological synapse. Nat. Immunol. *4*, 1111–1120.

Cole, T. B., Wenzel, H. J., Kafer, K. E., Schwartzkroin, P. A., and Palmiter, R. D. (1999). Elimination of zinc from synaptic vesicles in the intact mouse brain by disruption of the ZnT3 gene. Proc. Natl. Acad. Sci. USA *96*, 1716–1721.

Darnell, R. B., Furneaux, H. M., and Posner, J. B. (1991). Antiserum from a patient with cerebellar degeneration identifies a novel protein in Purkinje cells, cortical neurons, and neuroectodermal tumors. J. Neurosci. *11*, 1224–1230.

Dell'Angelica, E. C., Mullins, C., Caplan, S., and Bonifacino, J. S. (2000). Lysosome-related organelles. FASEB J. *14*, 1265–1278.

Dell'Angelica, E. C., Ohno, H., Ooi, C. E., Rabinovich, E., Roche, K. W., and Bonifacino, J. S. (1997a). AP-3, an adaptor-like protein complex with ubiquitous expression. EMBO J. *16*, 917–928.

Dell'Angelica, E. C., Ooi, C. E., and Bonifacino, J. S. (1997b). Beta3A-adaptin, a subunit of the adaptor-like complex AP-3. J. Biol. Chem. *272*, 15078–15084.

Faundez, V., Horng, J. T., and Kelly, R. B. (1998). A function for the AP3 coat complex in synaptic vesicle formation from endosomes. Cell *93*, 423–432.

Faundez, V., and Kelly, R. B. (2000). The AP-3 complex required for endosomal synaptic vesicle biogenesis is associated with a casein kinase I alpha-like isoform. Mol. Biol. Cell *11*, 2591–2604.

Feng, L., *et al*. (1999). The beta3A subunit gene (Ap3b1) of the AP-3 adaptor complex is altered in the mouse hypopigmentation mutant pearl, a model for Hermansky-Pudlak syndrome and night blindness. Hum. Mol. Genet. *8*, 323–330.

Folsch, H., Ohno, H., Bonifacino, J. S., and Mellman, I. (1999). A novel clathrin adaptor complex mediates basolateral targeting in polarized epithelial cells. Cell *99*, 189–198.

Folsch, H., Pypaert, M., Maday, S., Pelletier, L., and Mellman, I. (2003). The AP-1A and AP-1B clathrin adaptor complexes define biochemically and functionally distinct membrane domains. J. Cell Biol. *163*, 351–362.

Folsch, H., Pypaert, M., Schu, P., and Mellman, I. (2001). Distribution and function of AP-1 clathrin adaptor complexes in polarized epithelial cells. J. Cell Biol. *152*, 595–606.

Frederickson, C. J. (1989). Neurobiology of zinc and zinc-containing neurons. Int. Rev. Neurobiol. *31*, 145–238.

Frederickson, C. J., and Danscher, G. (1990). Zinc-containing neurons in hippocampus and related CNS structures. Prog. Brain Res. *83*, 71–84.

Gan, Y., McGraw, T. E., and Rodriguez-Boulan, E. (2002). The epithelial-specific adaptor AP1B mediates post-endocytic recycling to the basolateral membrane. Nat. Cell Biol. *4*, 605–609.

He, G., Gupta, S., Yi, M., Michaely, P., Hobbs, H. H., and Cohen, J. C. (2002). ARH is a modular adaptor protein that interacts with the LDL receptor, clathrin, and AP-2. J. Biol. Chem. *277*, 44044–44049.

Huang, P., Liu, J., Di, A., Robinson, N. C., Musch, M. W., Kaetzel, M. A., and Nelson, D. J. (2001). Regulation of human CLC-3 channels by multifunctional Ca2+/calmodulin-dependent protein kinase. J. Biol. Chem. *276*, 20093–20100.

Janvier, K., Kato, Y., Boehm, M., Rose, J. R., Martina, J. A., Kim, B. Y., Venkatesan, S., and Bonifacino, J. S. (2003). Recognition of dileucine-based sorting signals from HIV-1 Nef and LIMP-II by the AP-1 gamma-sigma1 and AP-3 delta-sigma3 hemicomplexes. J. Cell Biol. *163*, 1281–1290.

Kantheti, P., Diaz, M. E., Peden, A. E., Seong, E. E., Dolan, D. F., Robinson, M. S., Noebels, J. L., and Burmeister, M. L. (2003). Genetic and phenotypic analysis of the mouse mutant mh(2J), an Ap3d allele caused by IAP element insertion. Mamm. Genome *14*, 157–167.

Kantheti, P., *et al*. (1998). Mutation in AP-3 delta in the mocha mouse links endosomal transport to storage deficiency in platelets, melanosomes, and synaptic vesicles. Neuron *21*, 111–122.

Kim, Y. M., and Benovic, J. L. (2002). Differential roles of arrestin-2 interaction with clathrin and adaptor protein 2 in G protein-coupled receptor trafficking. J. Biol. Chem. *277*, 30760–30768.

Kontgen, F., Suss, G., Stewart, C., Steinmetz, M., and Bluethmann, H. (1993). Targeted disruption of the MHC class II Aa gene in C57BL/6 mice. Int. Immunol. *5*, 957–964.

Laporte, S. A., Miller, W. E., Kim, K. M., and Caron, M. G. (2002). beta-Arrestin/AP-2 interaction in G protein-coupled receptor internalization: identification of a beta-arrestin binging site in beta 2-adaptin. J. Biol. Chem. *277*, 9247–9254.

Laporte, S. A., Oakley, R. H., Holt, J. A., Barak, L. S., and Caron, M. G. (2000). The interaction of beta-arrestin with the AP-2 adaptor is required for the clustering of beta 2-adrenergic receptor into clathrin-coated pits. J. Biol. Chem. *275*, 23120–23126.

Li, X., Wang, T., Zhao, Z., and Weinman, S. A. (2002). The ClC-3 chloride channel promotes acidification of lysosomes in Chinese hamster ovary-K1 and Huh-7 cells. Am. J. Physiol. *282*, C1483–C1491.

Meberg, P. J., and Miller, M. W. (2003). Culturing hippocampal and cortical neurons. Methods Cell Biol. *71*, 111–127.

Mishra, S. K., Watkins, S. C., and Traub, L. M. (2002). The autosomal recessive hypercholesterolemia (ARH) protein interfaces directly with the clathrin-coat machinery. Proc. Natl. Acad. Sci. USA *99*, 16099–16104.

Nakagawa, T., Setou, M., Seog, D., Ogasawara, K., Dohmae, N., Takio, K., and Hirokawa, N. (2000). A novel motor, KIF13A, transports mannose-6-phosphate receptor to plasma membrane through direct interaction with AP-1 complex. Cell *103*, 569–581.

Nakatsu, F., *et al*. (2004). Defective function of GABA-containing synaptic vesicles in mice lacking the AP-3B clathrin adaptor. J. Cell Biol. *167*, 293–302.

Newman, L. S., McKeever, M. O., Okano, H. J., and Darnell, R. B. (1995). Beta-NAP, a cerebellar degeneration antigen, is a neuron-specific vesicle coat protein. Cell *82*, 773–783.

Ohno, H., Aguilar, R. C., Yeh, D., Taura, D., Saito, T., and Bonifacino, J. S. (1998). The medium subunits of adaptor complexes recognize distinct but overlapping sets of tyrosine-based sorting signals. J. Biol. Chem. *273*, 25915–25921.

Palmiter, R. D., Cole, T. B., Quaife, C. J., and Findley, S. D. (1996). ZnT-3, a putative transporter of zinc into synaptic vesicles. Proc. Natl. Acad. Sci. USA *93*, 14934–14939.

Peden, A. A., Oorschot, V., Hesser, B. A., Austin, C. D., Scheller, R. H., and Klumperman, J. (2004). Localization of the AP-3 adaptor complex defines a novel endosomal exit site for lysosomal membrane proteins. J. Cell Biol. *164*, 1065–1076.

Peden, A. A., Rudge, R. E., Lui, W. W., and Robinson, M. S. (2002). Assembly and function of AP-3 complexes in cells expressing mutant subunits. J. Cell Biol. *156*, 327–336.

Pevsner, J., Volknandt, W., Wong, B. R., and Scheller, R. H. (1994). Two rat homologs of clathrin-associated adaptor proteins. Gene *146*, 279–283.

Robinson, M. S. (2004). Adaptable adaptors for coated vesicles. Trends Cell Biol. *14*, 167–174.

Salazar, G., Love, R., Styers, M. L., Werner, E., Peden, A., Rodriguez, S., Gearing, M., Wainer, B. H., and Faundez, V. (2004a). AP-3-dependent mechanisms control the targeting of a chloride channel (ClC-3) in neuronal and non-neuronal cells. J. Biol. Chem. *279*, 25430–25439.

Salazar, G., Love, R., Werner, E., Doucette, M. M., Cheng, S., Levey, A., and Faundez, V. (2004b). The zinc transporter ZnT3 interacts with AP-3 and it is preferentially targeted to a distinct synaptic vesicle subpopulation. Mol. Biol. Cell *15*, 575–587.

Salem, N., Faundez, V., Horng, J. T., and Kelly, R. B. (1998). A v-SNARE participates in synaptic vesicle formation mediated by the AP3 adaptor complex. Nat. Neurosci. *1*, 551–556.

Seong, E., Saunders, T. L., Stewart, C. L., and Burmeister, M. (2004). To knockout in 129 or in C57BL/ *6*, that is the question. Trends Genet. *20*, 59–62.

Simpson, F., Bright, N. A., West, M. A., Newman, L. S., Darnell, R. B., and Robinson, M. S. (1996). A novel adaptor-related protein complex. J. Cell Biol. *133*, 749–760.

Simpson, F., Peden, A. A., Christopoulou, L., and Robinson, M. S. (1997). Characterization of the adaptor-related protein complex, AP-3. J. Cell Biol. *137*, 835–845.

Sloviter, R. S. (1982). A simplified Timm stain procedure compatible with formaldehyde fixation and routine paraffin embedding of rat brain. Brain Res. Bull. *8*, 771–774.

Stobrawa, S. M., *et al*. (2001). Disruption of ClC-3, a chloride channel expressed on synaptic vesicles, leads to a loss of the hippocampus. Neuron *29*, 185–196.

Styers, M. L., Salazar, G., Love, R., Peden, A. A., Kowalczyk, A. P., and Faundez, V. (2004). The endo-lysosomal sorting machinery interacts with the intermediate filament cytoskeleton. Mol. Biol. Cell *15* (*in press*).

Swiatek, P. J., and Gridley, T. (1993). Perinatal lethality and defects in hindbrain development in mice homozygous for a targeted mutation of the zinc finger gene Krox20. Genes Dev. *7*, 2071–2084.

Takatsu, H., Sakurai, M., Shin, H. W., Murakami, K., and Nakayama, K. (1998). Identification and characterization of novel clathrin adaptor-related proteins. J. Biol. Chem. *273*, 24693–24700.

Wenzel, H. J., Cole, T. B., Born, D. E., Schwartzkroin, P. A., and Palmiter, R. D. (1997). Ultrastructural localization of zinc transporter-3 (ZnT-3) to synaptic vesicle membranes within mossy fiber boutons in the hippocampus of mouse and monkey. Proc. Natl. Acad. Sci. USA *94*, 12676–12681.

Yang, W., Li, C., Ward, D. M., Kaplan, J., and Mansour, S. L. (2000). Defective organellar membrane protein trafficking in Ap3b1-deficient cells. J. Cell Sci. *113*, 4077–4086.

Zakharenko, S., Chang, S., O'Donoghue, M., and Popov, S. V. (1999). Neurotransmitter secretion along growing nerve processes: comparison with synaptic vesicle exocytosis. J. Cell Biol. *144*, 507–518.